# Constraining global isoprene emissions with Global Ozone Monitoring Experiment (GOME) formaldehyde column measurements

Changsub Shim, Yuhang Wang, and Yunsoo Choi
Department of Earth and Atmospheric Sciences, Georgia Institute of Technology, Atlanta, Georgia, USA

Paul I. Palmer and Dorian S. Abbot
Department of Earth and Planetary Sciences and Division of Engineering and Applied Sciences, Harvard University, Cambridge, Massachusetts, USA

Kelly Chance
Harvard-Smithsonian Center for Astrophysics, Cambridge, Massachusetts, USA

[1]   Biogenic isoprene plays an important role in tropospheric chemistry. Current isoprene emission estimates are highly uncertain because of a lack of direct observations. Formaldehyde (HCHO) is a high-yield product of isoprene oxidation. The short photochemical lifetime of HCHO allows the observation of this trace gas to help constrain isoprene emissions. We use HCHO column observations from the Global Ozone Monitoring Experiment (GOME). These global data are particularly useful for studying large isoprene emissions from the tropics, where in situ observations are sparse. Using the global Goddard Earth Observing System–Chemistry (GEOS-CHEM) chemical transport model as the forward model, a Bayesian inversion of GOME HCHO observations from September 1996 to August 1997 is conducted to calculate global isoprene emissions. Column contributions to HCHO from 10 biogenic sources, in addition to biomass-burning and industrial sources, are considered. The inversion of these 12 HCHO sources is conducted separately for eight geographical regions (North America, Europe, east Asia, India, Southeast Asia, South America, Africa, and Australia). GOME measurements with high signal-to-noise ratios are used. The a priori simulation greatly underestimates global HCHO columns over the eight geographical regions (bias, $-14$ to $-46\%$; $R = 0.52-0.84$). The a posteriori solution shows generally higher isoprene and biomass-burning emissions, and these emissions reduce the model biases for all regions (bias, $-3.6$ to $-25\%$; $R = 0.56-0.84$). The negative bias in the a posteriori estimate reflects in part the uncertainty in GOME measurements. The a posteriori estimate of the annual global isoprene emissions of 566 Tg C yr$^{-1}$ is $\sim$50% larger than the a priori estimate. This increase of global isoprene emissions significantly affects tropospheric chemistry, decreasing the global mean OH concentration by 10.8% to $0.95 \times 10^6$ molecules/cm$^3$. The atmospheric lifetime of $CH_3CCl_3$ increases from 5.2 to 5.7 years.

**Citation:** Shim, C., Y. Wang, Y. Choi, P. I. Palmer, D. S. Abbot, and K. Chance (2005), Constraining global isoprene emissions with Global Ozone Monitoring Experiment (GOME) formaldehyde column measurements, *J. Geophys. Res.*, *110*, D24301, doi:10.1029/2004JD005629.

## 1.  Introduction

[2]   Volatile organic compounds (VOCs) play an important role in oxidation chemistry in the troposphere [*Chameides et al.*, 1992; *Moxim et al.*, 1996; *Houweling et al.*, 1998; *Wang et al.*, 1998b; *Poisson et al.*, 2000]. Biogenic emissions are major sources of VOCs [e.g., *Zimmerman*, 1979; *Lamb et al.*, 1987; *Mueller*, 1992]. Isoprene, in particular, represents almost half of the total source of biogenic VOCs, and almost 40% of total VOC emissions on a global scale [*Guenther et al.*, 1995]. Furthermore, the formation of secondary organic aerosols via photooxidation of isoprene affects the global climate [*Limbeck et al.*, 2003; *Claeys et al.*, 2004].

[3]   Isoprene emissions depend on vegetation types, light intensity, temperature and leaf area index (LAI) [*Lamb et al.*, 1987; *Guenther et al.*, 1995]. Global emissions of isoprene are generally estimated by extrapolating from limited laboratory and field measurements to the prescribed global ecosystems. Various emission parameterizations have been proposed [e.g., *Lamb et al.*, 1987; *Guenther et al.*,

1995]. Despite these efforts, large uncertainties still remain in the estimates [*Hewitt and Street*, 1992; *Guenther et al.*, 1995]. The difficulty lies in the scarcity of direct measurements. The problem is most acute for tropical ecosystems [*Guenther et al.*, 1995; *Pierce et al.*, 1998], which collectively account for more than half of global isoprene emissions [*Guenther et al.*, 1995].

[4] Formaldehyde is a product of VOC oxidation. The main sinks of HCHO are photolysis and the reaction with atmospheric OH, and its lifetime against oxidation (on the order of hours) is short enough not to be significantly affected by transport. Methane is an important HCHO source, but it is well mixed in the troposphere because of its long lifetime. Methane oxidation provides the background HCHO levels.

[5] Previously, isoprene emissions over North America in summer have been derived using HCHO column measurements from the Global Ozone Monitoring Experiment (GOME) [*Chance et al.*, 2000; *Palmer et al.*, 2003a; *Abbot et al.*, 2003]. It was found that isoprene is the dominant contributor to HCHO over North America in the growing season; the enhancements above the $CH_4$-oxidation-induced background levels are generally linear with local isoprene emissions over North America [*Chance et al.*, 2000; *Palmer et al.*, 2003a]. Using that information, the seasonal and interannual variations in GOME HCHO columns over North America has been investigated [*Abbot et al.*, 2003]. Here we extend these previous studies to the global scale and we also explicitly consider isoprene emissions from 10 vegetation groups to capture the large difference in base emissions for different types of vegetations. The sources from biomass burning and industry are also treated separately.

[6] In this work, we apply GOME observations of HCHO column from September 1996 to August 1997 to constrain global isoprene emissions. In order to obtain best estimations of isoprene emissions, we use statistical inferences to fit the model simulated HCHO column concentrations toward GOME-observed HCHO column concentrations (inverse modeling). To minimize the effects of GOME measurement uncertainties, we selected eight regions with high signal-to-noise ratios (the ratio of slant column to signal fitting error >4). These regions are located over North America, Europe, east Asia, India, Southeast Asia, South America, Africa, and Australia.

[7] Model parameters (state vector) considered for the HCHO sources include the oxidation of isoprene from nine major vegetation groups; the tenth group includes isoprene from all other vegetation types and biogenic VOCs other than isoprene. The other two HCHO sources considered are biomass burning (combined with biofuel burning) and industry. The sources include primary emissions of HCHO and secondary chemical production during the oxidation of other VOCs.

[8] Uncertainties of model source parameters and GOME measurements are taken into account through Bayesian inverse modeling [*Rodgers*, 2000] to produce the a posteriori global isoprene emissions. The global Goddard Earth Observing System–Chemistry (GEOS-CHEM) chemical transport model [*Bey et al.*, 2001] is used for the a priori estimate. We conduct for each region an inversion of 12 different source types using monthly mean observations during growing seasons. The effects of a posteriori change of isoprene emissions on global $O_3$ and OH are estimated.

## 2. HCHO as a Proxy for Isoprene Emissions

[9] The HCHO yield from isoprene oxidation on a per carbon basis is in the range of 0.3–0.45; it increases with $NO_X$ concentrations [*Horowitz et al.*, 1998; *Palmer et al.*, 2003a]. *Palmer et al.* [2003a] discussed the robustness of the isoprene oxidation chemical mechanism in the model over North America in July 1996. They did not include the kinetics uncertainty in their inversion calculation. We assume in this work that this uncertainty in the estimated HCHO yield is small compared to GOME retrieval errors, which are fairly large (section 3). Quantitative assessment of the kinetics uncertainty with critical laboratory measurements is beyond the scope of this work.

[10] Formaldehyde can be produced within an hour from isoprene emissions because the lifetime of isoprene is about 0.5 hour during late morning. The corresponding lifetimes of major secondary products of isoprene oxidation are about 1.5–2.5 hours [*Carslaw et al.*, 2000]. At GOME measurement time of 1030 local time (LT), the impact of secondary products is also mitigated by the relatively weak isoprene emissions before the measurement time due to less light intensity and lower temperature. At surface wind speed of 0–10 m/s, the transport distance of secondary products is <150 km since 0630 LT, much less than the model grid size (4° × 5°). Thus the relatively short lifetimes of isoprene, its major secondary products, and HCHO render the effect of transport insignificant in a coarse-resolution model. The isoprene oxidation with $O_3$ is insignificant because the reaction is much slower than that with OH and the HCHO yield is small (<0.2) [*Atkinson*, 1994]. The per-carbon HCHO yields from larger biogenic VOCs, such as monoterpenes, are known to be much less than that of isoprene because of the efficient aerosol uptake of the oxidation products [*Kamens et al.*, 1982; *Hatakeyama et al.*, 1991; *Orlando et al.*, 2000; *Palmer et al.*, 2003a]. Methanol ($CH_3OH$), the other main biogenic HCHO source, has a much longer lifetime (several days). Formaldehyde from $CH_3OH$ oxidation is distributed over large regions relative to the model grid size [*Palmer et al.*, 2003a].

[11] Industrial VOCs including alkanes, alkenes, and aromatics contribute less to HCHO than isoprene during growing seasons. The lifetimes of alkenes are generally longer than that of isoprene [*Atkinson*, 1994] and those of alkanes are much longer [*Atkinson*, 1994]. Therefore HCHO from these VOCs are distributed over large regions. During growing seasons, their contributions to HCHO are relatively small over the regions with substantial biogenic isoprene emissions (to be shown in Table 3). The latter regions are the focus of our inverse modeling. The HCHO yields of aromatics are generally very small (less than a few percent) [*Dumdei et al.*, 1988]. Therefore the impact of those species is not important in this study.

[12] Methane oxidation has a yield of about 1 HCHO per unit carbon and $CH_4$ is well mixed in the atmosphere because of its long lifetime (~10 years). Its contribution of about 30% to HCHO column defines the atmospheric HCHO background concentrations [*Palmer et al.*, 2003a]. Recent studies [*Palmer et al.*, 2003a; *Abbot et al.*, 2003]
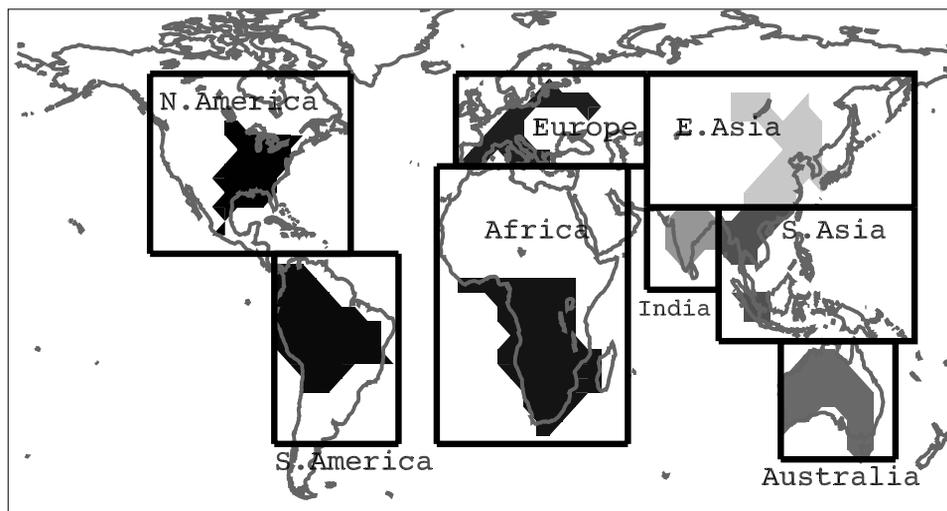
**Figure 1.** Inverse modeling regions with high signal-to-noise ratios in GOME HCHO column measurements are shown by shaded areas. The a posteriori source parameters (state vector) are applied to the rectangle regions in order to estimate the global a posteriori isoprene emissions.

show that the variability of HCHO columns at northern midlatitudes reflects the production from isoprene oxidation. On a global scale, the variability of HCHO columns is also mostly affected by emissions and photochemistry over the regions of interest.

## 3. GOME HCHO Column Measurements and the Uncertainties

[13] GOME is on board the ERS-2 satellite launched in 1995 to monitor atmospheric trace gases. It measures solar backscattered radiances with spectral resolutions of 0.2–0.4 nm in a relatively wide spectral range (237–794 nm, UV to near IR) [*Burrows et al.*, 1999]. The satellite moves in descending node passing the equator at 1030 LT in a Sun-synchronous orbit. In the nadir-viewing mode, it has a $32°$ across-track scan angle. It has a spatial resolution of $40 \times 320 \text{ km}^2$ and takes $\sim$3 days to cover the globe. The HCHO absorption spectra at 337–356 nm are fitted to reference spectra to determine slant columns with a fitting uncertainty of $4.0 \times 10^{15}$ molecules $\text{cm}^{-2}$ [*Chance et al.*, 2000].

[14] In our analysis, the GOME data that have cloud fraction >40% are excluded using an improved GOME cloud product, the GOME Cloud Algorithm (GOMECAT) [*Kurosu et al.*, 1999]. The GOME measurements are affected by the South Atlantic Anomaly (SAA), where radiation is exceptionally strong because of the anomaly of the Earth magnetic field [*Heirtzler*, 2002]. (The region will be shown in Figure 4.) We do not include the region in inverse modeling.

[15] In order to convert slant columns to vertical columns, air mass factors (AMFs) are calculated by a radiative transfer model (LIDORT) [*Spurr*, 2002] with the vertical profiles of HCHO taken from the GEOS-CHEM simulation [*Palmer et al.*, 2001; *Martin et al.*, 2002]. The sources of uncertainty in the AMF calculation are due to the uncertainties in UV albedo, vertical distribution of HCHO, and aerosols. Following the work by *Palmer et al.* [2001] and *Martin et al.* [2002], we calculate the AMF uncertainties, which are in the range of $1.0–13 \times 10^{15}$ molecules $\text{cm}^{-2}$.

[16] The GOME instrument is affected by a diffuser plate problem, and it must be corrected in data retrieval [*Martin et al.*, 2002; *Palmer et al.*, 2003a]. As a result of that artifact, HCHO columns over the remote ocean can be much higher than the background levels due to methane oxidation ($<5.0 \times 10^{15}$ molecules $\text{cm}^{-2}$) [*Abbot et al.*, 2003]. In order to correct the artifact, *Martin et al.* [2002] and *Palmer et al.* [2003a] used the following procedure. First, subtract the mean HCHO column over the Pacific from the corresponding GOME column for each latitude band. Second, add GEOS-CHEM-simulated HCHO columns over the Pacific to GOME columns. The difference between GOME and simulated HCHO columns over the Pacific reflects the errors due to the diffuser plate artifact.

[17] When applying the same procedure, we find high HCHO variability and noise over the Atlantic, Indian, and Southern Oceans (not shown). Instead of assuming that the HCHO columns over the Pacific represent background concentrations, we calculate the background HCHO column for each latitude band as the value at the lower 20th percentile. We subtract the background column from GOME HCHO column and then add the 20th percentile value from GEOS-CHEM for each latitude band on a daily basis. In addition to the above procedure, we exclude the data that have slant column uncertainties greater than $2\sigma$ ($\sigma$ is the HCHO fitting uncertainty of $4.0 \times 10^{15}$ molecules $\text{cm}^{-2}$) because these data are usually associated with large HCHO variability over the ocean. We find that the new procedure results in much lower GOME HCHO variability over the oceans. The magnitude of this correction is about $2 \times 10^{15}$ molecules $\text{cm}^{-2}$ and the corresponding uncertainty is about $8 \times 10^{14}$ molecules $\text{cm}^{-2}$. The vertical columns with 20th percentile corrections are about 10% less than those with the Pacific mean corrections. Taking into account these uncertainties, we obtain the overall GOME HCHO retrieval uncertainty in the range of $6–15 \times 10^{15}$ molecules $\text{cm}^{-2}$ (or 53–69%, to be shown in Table 2).

[18] In inverse modeling, we consider only the regions with relatively high signal-to-noise ratios in GOME measurements. Over these regions, daily GOME HCHO slant

columns are >4σ (1.6 × 10^{16} molecules cm^{-2}) and the observations satisfying this condition must be available for more than a season. This criterion is applied for defining the regions for inverse modeling. Shown in Figure 1 are such determined source regions over North America (eastern United States), Europe (western Europe), East Asia, India, Southeast Asia, South America (Amazon), Africa, and Australia. For the regions at midlatitudes, only during the growing season (May–August) do GOME measurements meet the data selection criterion. As previously stated, the SAA region is not included. The northern equatorial Africa (4°–12°N) was not included in inverse modeling for reasons described in section 5.2.9.

# 4. Model Description and Applications

## 4.1. GEOS-CHEM Model

[19] GEOS-CHEM is a global 3-D chemical transport model driven by assimilated meteorological data (GEOS-STRAT for 1996–1997) from the Global Modeling Assimilation Office (GMAO) [*Schubert et al.*, 1993]. The 3-D meteorological fields are updated every 6 hours, and the surface fields and mixing depths are updated every 3 hours. We use version 5.05 here with a horizontal resolution of 4° × 5° and 26 vertical layers. GEOS-CHEM includes a comprehensive tropospheric $O_3$-$NO_x$-VOC chemical mechanism [*Bey et al.*, 2001], which includes the oxidation mechanisms of six VOCs (ethane, propane, lumped >$C_3$ alkanes, lumped >$C_2$ alkenes, isoprene, and terpenes). In the a priori and a posteriori simulations, the model was spun up for a year and the second year's results are used.

[20] Isoprene emissions are estimated using the algorithm of *Guenther et al.* [1995] with updates [*Wang et al.*, 1998a; *Bey et al.*, 2001]. The global vegetation distribution of 73 ecosystem types is from *Olson* [1992]. A GEOS-CHEM grid (4° × 5°) contains a maximum of 15 ecosystem types, each of which has its own area fraction and base emission. The seasonality is determined by light intensity, temperature, and LAI. The LAI values are based on satellite observations [*Wang et al.*, 1998a]. The seasonal cycle of light intensity is largely a function of month. We found that the seasonal cycles of GEOS-STRAT surface temperature in some regions led to disagreement with the observations (section 5.2). *Bey et al.* [2001] reduced base isoprene emission rates for several tropical ecosystems (tropical rain forest, tropical montane, tropical seasonal forest, and drought deciduous) and for grass/shrub by a factor of 3 on the basis of available measurements of isoprene concentrations and fluxes [*Helmig et al.*, 1998; *Klinger et al.*, 1998]. We here use the updates by *Bey et al.* [2001]. The resulting global isoprene source during September 1996 to August 1997 is 375 Tg C yr^{-1} (397 Tg C yr^{-1} in 1994 [*Bey et al.*, 2001]).

[21] GEOS-CHEM uses the emission inventories of industrial $NO_X$ and VOCs for 1985 by *Wang et al.* [1998a]. Those emissions are scaled for specific years with national emission data [*Bey et al.*, 2001]. Biomass-burning emissions of CO are constrained by satellite observations of fire counts from the Along Track Scanning Radiometer (ATSR) and advanced very high resolution radiometer (AVHRR), and Aerosol Index (AI) from Total Ozone Mapping Spectrometer (TOMS) [*Duncan et al.*, 2003]. Biomass-burning

emissions of $NO_X$ and VOCs are derived by applying their emission ratios to CO [*Wang et al.*, 1998a]. We use HCHO/CO molar emission ratios by *Andreae and Merlet* [2001] as a function of fuel type. The average emission ratio is 0.01. The primary biomass-burning emission of HCHO accounts for about 22% of total VOC emissions from biomass burning in the model. The GEOS-CHEM-simulated HCHO columns are sampled along the GOME orbit tracks at the GOME observation time (1000–1100 LT) on a daily basis. However, we conduct inverse modeling of monthly averages since GOME HCHO columns have a large day-to-day variability, which is not captured by GEOS-CHEM [e.g., *Palmer et al.*, 2003a].

## 4.2. Inverse Modeling

[22] We apply inverse modeling to estimate the source parameters of HCHO (state vector) using monthly GOME measurements with GEOS-CHEM as the forward model. The Bayesian least squares method is used [*Rodgers*, 2000]. The relationship between the observation vector **y** and state vector **x** can be described as

$$\mathbf{y} = \mathbf{Kx} + \varepsilon \qquad (1)$$

where the **K** matrix (Jacobian matrix) represents HCHO sensitivities to the state vector defined by the forward model, and $\varepsilon$ is the error term. The uncertainties are used for weightings of the observations and the a priori state vector. We consider the measurement and a priori model parameter errors. The a posteriori state vector $\hat{\mathbf{x}}$ is [*Rodgers*, 2000],

$$\hat{\mathbf{x}} = \mathbf{x_a} + \left(\mathbf{K^T S_\varepsilon^{-1} K} + \mathbf{S_a^{-1}}\right)^{-1} \mathbf{K^T S_\varepsilon^{-1}}(\mathbf{y} - \mathbf{Kx_a}) \qquad (2)$$

where $\mathbf{x_a}$ is the a priori state vector, $\mathbf{S_a}$ is the estimated error covariance matrix for $\mathbf{x_a}$, and $\mathbf{S_\varepsilon}$ is the error covariance matrix for observation errors. The a posteriori error covariance matrix is,

$$\hat{\mathbf{S}} = \left(\mathbf{K^T S_\varepsilon^{-1} K} + \mathbf{S_a^{-1}}\right)^{-1} \qquad (3)$$

[23] In inverse modeling, we consider 12 HCHO source parameters in the a priori state vector that contribute to HCHO column concentrations: isoprene emissions from 9 different vegetation groups, other biogenic VOCs including isoprene emissions from the rest of vegetation groups, and two additional HCHO sources from biomass burning and industry. Table 1 shows the global isoprene emissions estimates by *Guenther et al.* [1995] for the defined vegetation groups. Some vegetation groups are the major isoprene emitters for specific regions: agricultural lands for India, dry evergreen and crop/woods for Australia, and regrowing woods for North America. Figure 2 shows the global distribution of the vegetation groups.

[24] The measurement errors from GOME retrievals are discussed in section 3. As discussed in section 2, transport does not significantly affect GOME HCHO measurements used in inverse modeling, which are dominated by isoprene. Transport error is therefore not included in inverse modeling. The model parameter errors reflect the uncertainties of the source parameters in the forward model. We assign the source parameter errors for the vegetation types with field or

**Table 1.** Isoprene Emitting Ecosystem Groups Applied in Inverse Modeling[a]

| | Ecosystem Group | Olson Code | Global Emissions, Tg C yr$^{-1}$ | A Priori Uncertainty, % |
|---|---|---|---|---|
| 1 | tropical rain forest | 33 | 84.4 | 300 |
| 2 | grass/shrub (hot, cool) | 40, 41 | 91.7 | 400 |
| 3 | savanna | 43 | 48.3 | 400 |
| 4 | tropical seasonal forest and thorn woods | 29, 59 | 80.1 | 300 |
| 5 | temperate mixed and temperate deciduous | 24, 26 | 11.3 | 300 |
| 6 | agricultural lands | 31, 36 | 20.9 | 300 |
| 7 | dry evergreen and crop/woods (warm) | 48, 58 | 16.9 | 300 |
| 8 | regrowing woods | 56 | 27.5 | 300 |
| 9 | drought deciduous | 32 | 60.5 | 300 |
| 10 | rest of the ecosystems[b] | | 61.4 | 300 |
| Total | | | 503 | |

[a]Ecosystem types are defined by *Olson* [1992]. The global isoprene emissions are taken from *Guenther et al.* [1995].
[b]Includes all other ecosystems with biogenic emissions assigned by *Guenther et al.* [1995].

laboratory measurements to 300% [*Guenther et al.*, 1995], and to 400% for those without measurements. The assigned isoprene emission errors include all the variables in the model for estimating the natural VOC emissions [*Guenther et al.*, 1995]. The emissions of HCHO from biomass burning are calculated using the CO biomass-burning emission inventory and the HCHO/CO molar emission ratios. The CO biomass-burning emissions have an uncertainty of 50% [*Palmer et al.*, 2003b], while the HCHO/CO molar emission ratios as a function of fuel type were based on limited measurements compiled by *Andreae and Merlet* [2001]. Therefore we assume the uncertainty of HCHO emission from biomass burning is as high as that of isoprene (300%). We assign the error of 50% for industrial emissions [*Palmer et al.*, 2003b]. As stated in section 2.2, $CH_4$ provides the background source of HCHO. We do not include the $CH_4$ contributions in the inverse modeling because the uncertainty of HCHO from $CH_4$ oxidation is much smaller than that of isoprene emissions. Assigning the relatively small uncertainty to HCHO produced from $CH_4$ oxidation in inverse modeling results in no a posteriori change in this source.

[25] In the forward model calculations, we compute the sensitivity of HCHO columns to the emissions from the 12 source categories. The sensitivity calculation of HCHO columns to each source category is complicated by the feedbacks of these emissions on OH concentrations. When reducing isoprene emissions, OH concentrations increase affecting HCHO production and loss. In our calculations, we archive hourly OH, NO, and $O_3$ concentrations from the standard simulation. The sensitivity of HCHO columns to each source category is calculated by removing that source while holding hourly OH, NO, and $O_3$ concentrations to the values in the standard model. The procedure is necessary because the inverse model assumes that the Jacobian matrix is linear. The validity of the linear assumption is then
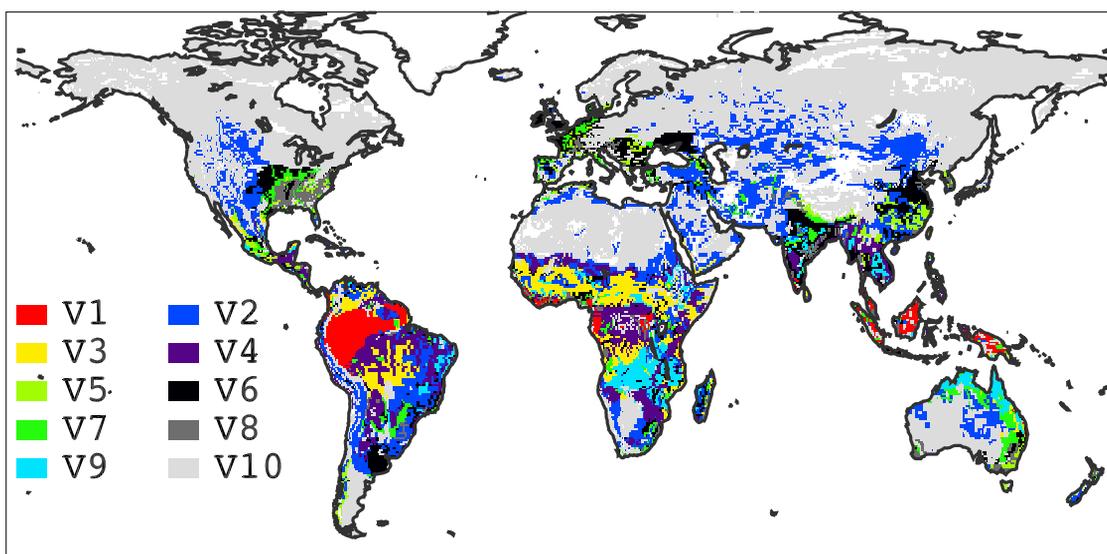


**Figure 2.** Global distribution of the 10 ecosystem groups (Table 1) applied in inverse modeling, including tropical rain forest (V1), grass/shrub (V2), savanna (V3), tropical seasonal forest and thorn woods (V4), temperate mixed and temperate deciduous (V5), agricultural lands (V6), dry evergreen and crop/woods (warm) (V7), regrowing woods (V8), drought deciduous (V9), and the rest of the ecosystems (V10). The ecosystem types are defined by *Olson* [1992] with a resolution of 0.5° × 0.5°.
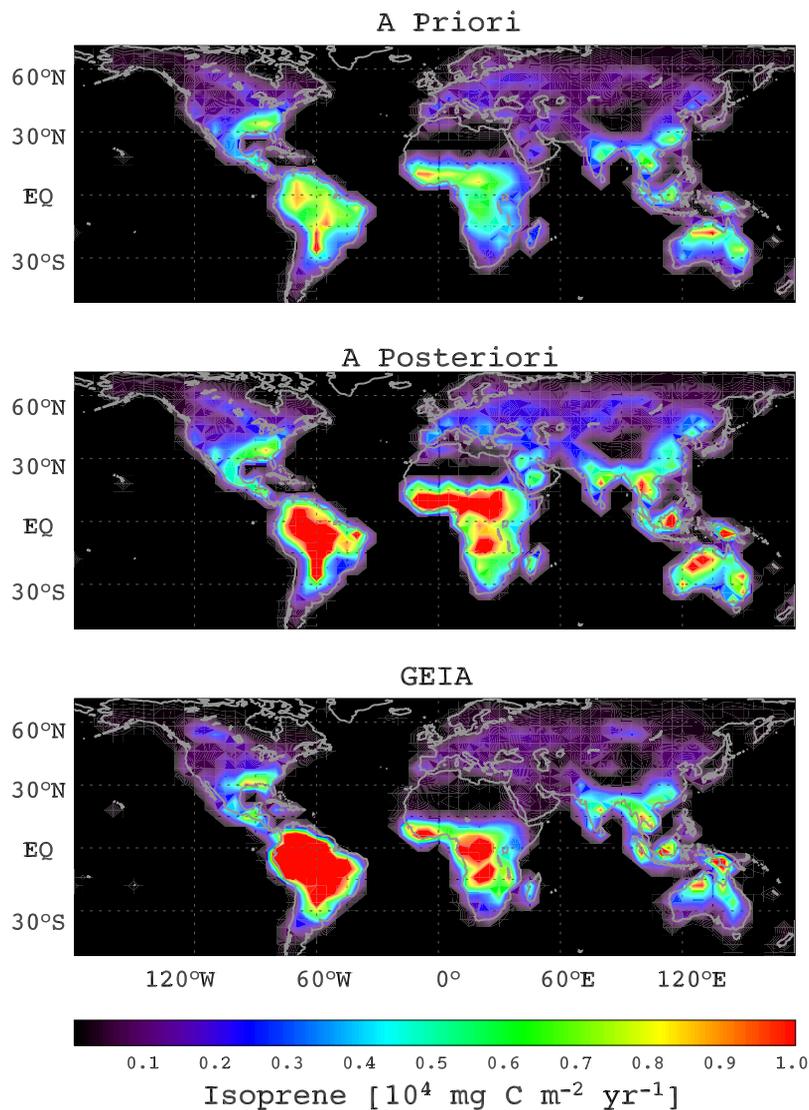
**Figure 3.** Estimated annual global distributions of isoprene emissions ($10^4$ mg C m$^{-2}$ yr$^{-1}$). (top) GEOS-CHEM simulation with the a priori isoprene emissions from September 1996 to August 1997. (middle) Same as top panel but with the a posteriori isoprene emissions. (bottom) GEIA inventory for 1990 [*Guenther et al.*, 1995].

checked by conducting a full chemistry simulation with the a posteriori sources and comparing the resulting HCHO columns with the linear projections by the inverse model (section 5.3). In this study, we find that the sensitivities of source parameters are close to linear in the range of emission variability for all eight regions with high signal-to-noise ratios in GOME HCHO measurements.

[26] We apply the inverse modeling to each region separately because the same vegetation types on different continents in the *Olson* [1992] map can have different species compositions (A. Guenther, personal communication, 2003). The regions for inverse modeling are shown in Figure 1. The selection of the significant source parameters in the state vector to avoid numerical errors in the inversion is described in section 5.3. In order to estimate the global a posteriori isoprene inventory, we extend a posteriori source parameters for isoprene for the eight regions (shaded

regions in Figure 1) to their respective continents between 40°S and 60°N where >95% of isoprene emissions take place (rectangle regions in Figure 1) by scaling each ecosystem emission with the a posteriori/a priori ratio of the corresponding source parameter (section 6).

## 5. Analysis

[27] The annual global distributions of isoprene for the GEIA 1990 inventory [*Guenther et al.*, 1995], and the September 1996 to August 1997 a priori and a posteriori GEOS-CHEM estimates are presented in Figure 3. The a posteriori isoprene emissions are increased (versus the a priori emissions) over all the regions, particularly over the tropics. Compared to the GEIA inventory, the a posteriori isoprene emissions are generally higher at midlatitudes but lower in the tropics. The exception is the much higher a

**Table 2.** Regional Statistics of GOME and Simulated HCHO Columns, and the a Priori, a Posteriori, and GEIA Estimates of the Annual Isoprene Emissions for the Inversion Regions[a]

| Regions | GOME $\Omega$,[b] % | Weighted Uncertainties[c] % | | Correlation Coefficient $R$[d] | | Model Bias, % | | Isoprene Emission, Tg C/yr | | |
|---|---|---|---|---|---|---|---|---|---|---|
| | | A Priori | A Posteriori | A Priori | A Posteriori | A Priori | A Posteriori | A Priori | A Posteriori | GEIA |
| North America | 59 | 291 | 69 | 0.84 | 0.84 | −14.3 | −3.6 | 22.2 | 25.7 | 21.4 |
| Europe | 69 | 287 | 96 | 0.52 | 0.60 | −29.9 | −11.9 | 9.5 | 12.0 | 6.1 |
| East Asia | 56 | 280 | 63 | 0.63 | 0.75 | −39.2 | −18.6 | 17.4 | 24.8 | 12.8 |
| India | 59 | 285 | 122 | 0.57 | 0.56 | −33.2 | −18.4 | 10.5 | 14.4 | 15.2 |
| Southeast Asia | 54 | 298 | 110 | 0.66 | 0.69 | −35.8 | −19.4 | 20.2 | 29.1 | 38.2 |
| South America | 54 | 337 | 75 | 0.58 | 0.64 | −31.8 | −12.6 | 79.4 | 106.4 | 163.5 |
| Africa | 53 | 332 | 102 | 0.56 | 0.54 | −46.3 | −23.6 | 60.3 | 103.3 | 105.7 |
| Australia | 69 | 302 | 96 | 0.52 | 0.56 | −40 | −24.8 | 33.3 | 50.6 | 31.1 |
| Global | 60 | | | 0.68 | | −35 | | 375 | 566 | 503 |

[a]The values are for the shaded area in Figure 1 during the growing seasons.
[b]$\Omega$ denotes the overall percentage GOME retrieval uncertainties with respect to the vertical columns.
[c]Weighted uncertainties of the state vector (source parameters).
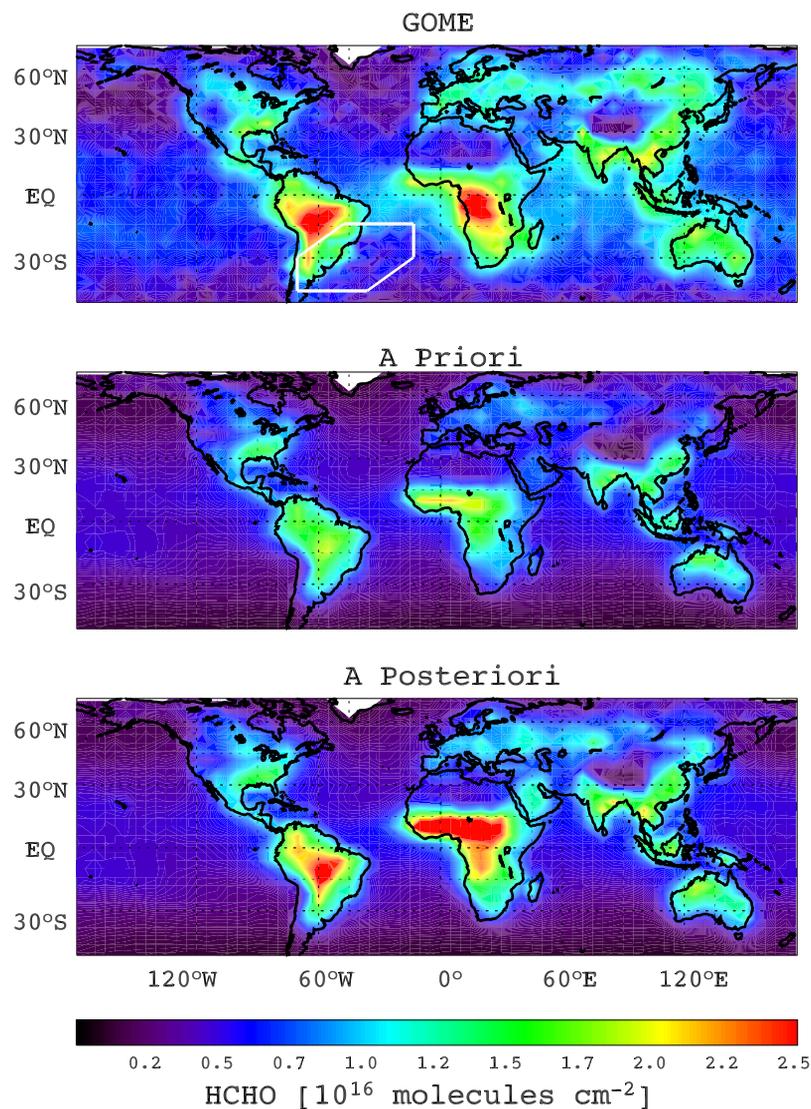[d]Calculated on the basis of $4° \times 5°$ monthly mean GOME and model data.



**Figure 4.** Annual mean observed and simulated vertical HCHO columns from September 1996 to August 1997. (top) GOME-retrieved columns. (middle) A priori GEOS-CHEM columns. (bottom) A posteriori GEOS-CHEM columns. The GEOS-CHEM HCHO columns shown are coincident in space and time with GOME measurements. The white polygon shows the region of the South Atlantic Anomaly.
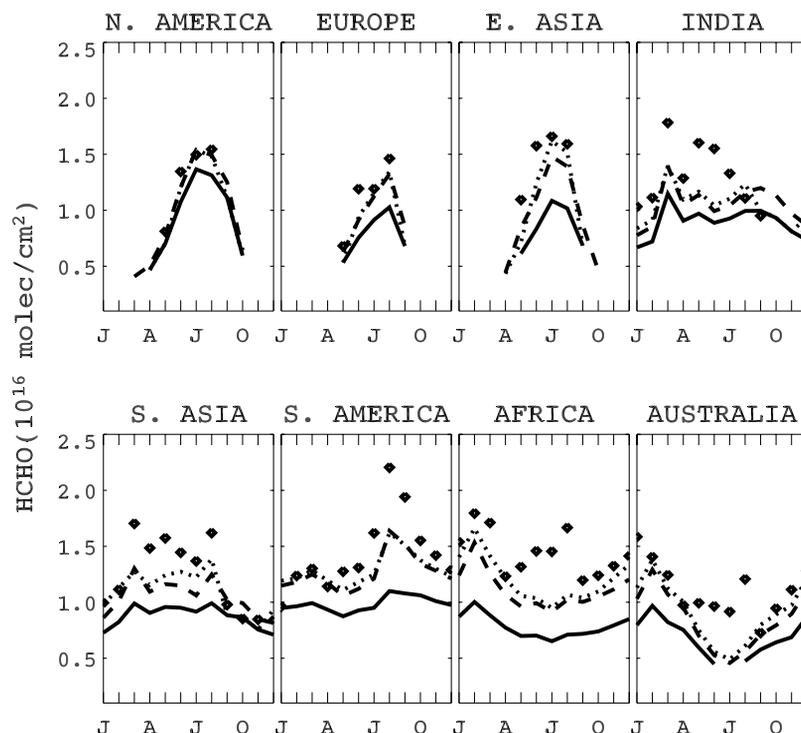
**Figure 5.** Monthly mean HCHO column concentrations in the eight regions (Figure 1) from September 1996 to August 1997. The time sequence is reordered to January through December. The diamonds show GOME column concentrations. The solid lines show the corresponding GEOS-CHEM-simulated columns with the a priori sources. The dashed lines are GEOS-CHEM-simulated columns with the a posteriori sources. The dotted lines show the linearly inverse-model-projected HCHO columns with the a posteriori sources. The values below the GOME detection limit ($4.0 \times 10^{15}$ molecules/cm$^2$) are not shown.

posteriori estimate over Australia. Table 2 shows the estimates of the annual isoprene emissions from the eight regions.

### 5.1. Observed and Simulated HCHO Columns

[28] The observed annual mean global HCHO columns from GOME and the corresponding columns simulated GEOS-CHEM with the a priori and a posteriori emissions are shown in Figure 4. The a priori GEOS-CHEM simulation significantly underestimates the global HCHO columns by >30%. The mean correlation coefficient between the a priori model simulation and GOME observations is 0.68. The discrepancies are particularly large over the tropical South America and Africa, where more than one third of global isoprene is emitted according to the a priori isoprene emissions.

[29] The uncertainties of GOME retrievals are large in the range of 53–69% over the eight selected regions, even though the regions are chosen on the basis of high signal-to-noise ratios. Table 2 shows the GOME uncertainty, correlation coefficient, and model bias for each region of inverse modeling. North America has the smallest bias (−14%) during the growing season (May–August). Africa has the largest bias (−46%).

[30] Figure 4 shows the annual mean GEOS-CHEM HCHO columns with a posteriori emissions. Full model simulations using the a posteriori emissions are in much better agreement with GOME observations over high-

isoprene regions. The regional biases of the a priori model are reduced by about 50% (Table 2). The a posteriori uncertainties are greatly reduced because of the constraints by GOME observations. The a posteriori model still has a low bias compared to GOME observations partly because of the relatively large GOME measurement uncertainties. Despite these improvements, there is still serious disagreement between GOME and a posteriori HCHO columns over northern equatorial Africa (Figure 4), which will be discussed in section 5.2.9.

### 5.2. Regional Isoprene Emissions

[31] Figure 5 compares simulated and observed GOME monthly column concentrations of HCHO over the eight selected regions (shaded regions in Figure 1). Table 3 shows the contribution by each emission category to both a priori GEOS-CHEM and a posteriori inverse-model-projected HCHO columns. The relative a posteriori changes of HCHO contributions from different vegetation groups are the same as those from isoprene emissions since the inversion is linear. We discuss the results by region in the following sections.

#### 5.2.1. North America (Eastern United States)

[32] We compare observed and simulated monthly HCHO columns ($4° \times 5°$) only for the growing season between May and August (section 3). The corresponding data correlation between a priori estimates and GOME observations is rather high. This correlation coefficient ($R$) of 0.84

**Table 3.** Mean Source Contributions to the a Priori and Inverse-Model-Projected HCHO Columns[a]

| | North America | | Europe | | East Asia | | India | | South Asia | | South America | | Africa | | Australia | |
|---|---|---|---|---|---|---|---|---|---|---|---|---|---|---|---|---|
| | Pri | Pos | Pri | Pos | Pri | Pos | Pri | Pos | Pri | Pos | Pri | Pos | Pri | Pos | Pri | Pos |
| V1 | -[b] | - | - | - | - | - | - | 1.5[c] | 5 | 7.9 | 13.8 | 17.9 | 2 | 6.4 | - | - |
| V2 | **6.1** | **8.5** | **2.3** | **5.4** | **8.1** | **21.8** | **2.5** | **6.5** | 1.6 | 1.6 | 8.6 | 4.3 | 2.7 | 10.3 | 4.8 | 2.9 |
| V3 | 1 | 1 | - | - | - | - | - | - | - | - | 15.6 | 21.4 | 10.5 | 14.6 | 1.2 | 5 |
| V4 | - | - | - | - | - | - | 4.6 | 6.9 | 8.5 | 16.2 | - | - | 4.5 | 4.5 | - | - |
| V5 | 7.8 | 13.3 | 5.7 | 10.3 | 12.5 | 1.3 | - | - | 3.2 | 4.8 | - | - | - | - | 1.6 | 1.6 |
| V6 | 5.6 | 8.9 | 4.8 | 16.3 | 4.9 | 12.8 | 8.3 | 7.4 | 4.9 | 14.3 | 1.2 | 1.2 | 2.1 | 2.1 | - | 1.8 |
| V7 | 4.6 | 3.2 | 1.2 | 2 | - | - | 1.9 | 1.9 | 1.2 | 1.2 | 2.6 | 2.6 | 1.4 | 1.4 | 14.5 | 10.1 |
| V8 | 22.6 | 18.1 | 3.7 | 4.1 | 1.3 | 5.2 | 7.5 | 13.5 | 8.3 | 8.3 | 1.6 | 1.6 | 3.4 | 3.4 | - | 5.9 |
| V9 | - | - | - | - | - | - | 2.4 | 3.4 | 3.5 | 1.7 | 1.8 | 1.6 | 6.9 | 15.2 | 4.3 | 4.7 |
| RV | 30.7 | 40 | 34.6 | 38 | 28.5 | 48.5 | 3.4 | 8.3 | 3.7 | 11.7 | 9.9 | 17.9 | 8.4 | 21.8 | 16.2 | 35.9 |
| BB | - | - | 1.8 | 1.8 | 3.4 | 14 | 9.9 | 10.8 | 5.6 | 11.3 | 2.3 | 11.3 | 4.2 | 8.8 | - | - |
| IND | 6 | 7.2 | 5.4 | 6.4 | 4.8 | 8.1 | 5.2 | 7.7 | 4.2 | 5.1 | 1 | 1 | 1.2 | 1.2 | - | - |
| Total | 125 | 141 | 90 | 115 | 98 | 146 | 88 | 108 | 89 | 118 | 98 | 129 | 78 | 121 | 67 | 91 |

[a]Units are $10^{14}$ molecules $cm^{-2}$. The inversion is applied for the individual region. All the inversion quantities here are for the shaded areas in Figure 1. We considered only the growing season (May–August) for the regions at midlatitudes. Ecosystem classification is from *Olson* [1992]. Inverse-model-projected HCHO columns are the products of the ratio of the a posteriori/a priori source parameters and the corresponding a priori HCHO columns. Pri, a priori emission contributions; Pos, a posteriori inverse model projections. V1–V9, isoprene contributions from tropical rain forest (V1), grass/shrub (V2), savanna (V3), tropical seasonal forest (V4), temperate mixed and temperate deciduous (V5), agricultural lands (V6), dry evergreen and crop/woods (V7), regrowing woods (V8), drought deciduous (V9), the rest of the biogenic sources (RV), biomass and biofuel burning (BB), and industrial VOC emissions (IND). "Total" also includes $CH_4$ oxidation.
[b]Values $<1.0 \times 10^{14}$ molec/$cm^2$.
[c]Boldface values denote that the vegetation types are included in the state vector. The number of state vectors for each region is listed in Table 4.

is comparable to the previous study (for July 1996) [*Palmer et al.*, 2003a]. According to the a priori estimate, regrowing woods is the largest isoprene emission group, and temperate mixed and temperate deciduous are the second largest group. The monthly contributions of the major a priori sources to HCHO columns are shown in Figure 6. The oxidation of $CH_4$ provides the background levels of HCHO columns ($\sim$25% of the total). The a priori biogenic emissions account for 63% of HCHO columns. The a posteriori source parameters suggest relatively small changes for most emission categories (Table 3), which implies that isoprene emissions over North America are relatively well estimated. The result is expected because the base emissions for vegetations in this region and Europe are better measured than over the other regions [*Guenther et al.*, 1995]. The a posteriori biogenic emissions of 26 Tg C $yr^{-1}$ in this region are about 15% higher and the resulting HCHO columns are in better agreement with GOME.

### 5.2.2. Europe

[33] This region has the a priori isoprene emissions of 9.5 Tg C $yr^{-1}$. As for North America, we consider only the growing season between May and August. The a priori biogenic emissions account for 58% of HCHO columns in that season (Table 3). The largest change in the a posteriori emissions is in those from agricultural lands. The inverse modeling results suggest an increase of this source by a factor of 3.4 (Table 3). Similarly large increases for this source category are found for east and Southeast Asia. It is possible that this problem is due to incorrect classification of vegetation types. Another possibility is that crop and farming practice over those regions are different from North America, resulting in different emissions. The total a posteriori isoprene source of 12 Tg C $yr^{-1}$ for the region is 26% higher than a priori (Table 2). The model bias improves from the a priori −29.9% to a posteriori −11.9%.

### 5.2.3. East Asia

[34] This region includes eastern China, Korea, and Japan with the a priori isoprene source of 17 Tg C $yr^{-1}$. The
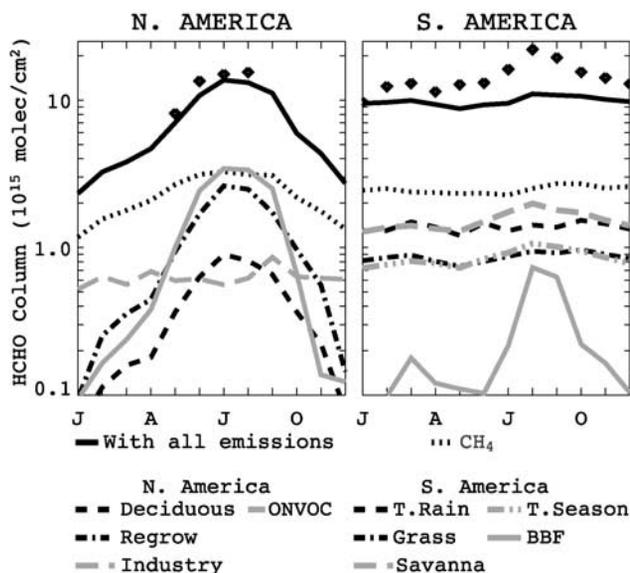


**Figure 6.** Contributions of the a priori sources to the simulated monthly mean HCHO column concentrations over North America (eastern United States) and South America (Amazon). The diamonds are GOME HCHO columns. "With all emissions" denotes the simulated HCHO column concentration with all emission sources. "$CH_4$" denotes HCHO from $CH_4$ oxidation. The other source contributions are "Deciduous" (temperate mixed and temperate deciduous), "ONVOC" (isoprene from the other ecosystems), "T. Rain" (tropical rain forest), "T. Season" (tropical seasonal forest and thorn woods), "Regrow" (regrowing woods), "Grass" (grass/shrub), and "BBF" (biomass and biofuel burning).

seasonal variation is similar to that of other northern midlatitude regions. We consider only the growing season (May–August) for inverse modeling. The a priori biogenic emissions account for 56% of HCHO columns in that season. Although the total isoprene source change is 43% (Table 2), large changes are found for individual sources including a factor of 2–4 increase in the emissions from grass/shrub, agricultural lands, and regrowing woods. The increase of the other biogenic sources is also significant. The emissions from mixed deciduous forests decrease by a factor of 10 (Table 3). These large changes appear to indicate problems in the *Olson* [1992] vegetation distribution. The a posteriori biomass-burning source of HCHO increases by a factor of 4 (Table 3), making it the most significant source in spring (not shown). After an increase of 43% in the a posteriori isoprene emissions to 24.8 Tg C yr$^{-1}$, the model is still biased low by 18.6% (Table 2).

### 5.2.4. India

[35] The rapid increase of GOME HCHO columns in March (Figure 5) coincides with biomass burning in this region. The model captures this seasonal change. However, the simulated biogenic emissions do not show the large increase from winter to summer as observed. Therefore the a posteriori model underestimates GOME HCHO columns in summer. The sources from industry and CH$_4$ oxidation do not have a large seasonal variation either. The most likely candidate to explain the seasonal change of GOME HCHO column is the biogenic sources. The current emission algorithm apparently does not simulate the seasonal cycle correctly. This region has the a priori isoprene emissions of 11 Tg C yr$^{-1}$. Inverse modeling suggests a factor 2–3 increase for isoprene emissions from grass/shrub, regrowing woods, and the rest of vegetation category. With an increase of 37% to 14.4 Tg C yr$^{-1}$, the model bias improves from the a priori −33.2% to a posteriori −18.4%.

### 5.2.5. Southeast Asia

[36] This region includes the Indochina Peninsula and Indonesia (4°S to 30°N) with the a priori isoprene source of 20 Tg C yr$^{-1}$. The biogenic emissions account for 40% of HCHO column concentrations. There are two features in the region that are similar to India. First, the large March maximum (Figure 5) is largely due to biomass-burning emissions. The inverse modeling suggests a factor of 2 increase of this source. Second, the observed large seasonal shift from winter to summer cannot be reproduced by the model. Large increases of isoprene emissions (by about a factor of 3) are needed for agriculture lands and the rest of vegetations group. The a posteriori isoprene emissions increase by 44% to 29.1 Tg C yr$^{-1}$and the model bias is reduced from the a priori −35.8% to a posteriori −19.4%.

### 5.2.6. South America (Amazon)

[37] This region including Amazon has a large source of isoprene (∼80 Tg C yr$^{-1}$), accounting for >20% of the global a priori source. Biogenic emissions account for 65% of the simulated HCHO column concentrations here. GOME HCHO observations show a distinct seasonal variation with a maximum in July–September (Figure 5). The simulated HCHO monthly columns are lower with a smaller seasonal variation. Figure 6 shows the source contributions of isoprene from tropical rain forest, tropical seasonal forest,

grass/shrub, savanna, and that from biomass burning. Among the major sources, the contributions from biomass-burning, savanna, and tropical seasonal forest emissions show the observed austral spring maximum. To capture the observed seasonal variation, the inverse modeling results suggest a factor of 5 increase in biomass burning, a factor of 2 increase in tropical seasonal forest emissions and a factor of 2 decrease in grass/shrub emissions. The posteriori isoprene emissions increase by 34% to 106 Tg C yr$^{-1}$, but are still 35% less than the corresponding GEIA estimate. The a posteriori model bias is decreased to −12.6%.

### 5.2.7. Africa

[38] This region (40°S to 4°N) has the a priori isoprene emissions of 60 Tg yr$^{-1}$. Biogenic emissions account for >50% of the model HCHO columns. The a priori simulation shows a large underestimate of the GOME observations (model bias, −46%). The inverse modeling results suggest large increases (a factor of 2–4) in emissions from tropical rain forest, grass/shrub, drought deciduous, and the other vegetation group. The HCHO source from biomass burning is increased by factor of 2 (Table 3). The a posteriori model reproduces reasonably well the seasonal increase from austral spring to summer due to increasing biogenic emissions, but fails to capture the high values in June–August. There are significant discrepancies between the simulated and GOME HCHO columns over northern equatorial Africa (Figure 5), where the model overestimates the observations. We investigate the causes in section 5.2.9. The inverse modeling shows a 71% increase of isoprene emissions 103.3 Tg C yr$^{-1}$ and the a posteriori model bias is decreased by 49% to −23.6%.

### 5.2.8. Australia

[39] This region (12°–40°S) shows a seasonal cycle typical for the Southern Hemisphere (Figure 5). Biogenic emissions account for 70% of the model HCHO columns. The a priori simulation greatly underestimates GOME observations in this region (−40%). The inverse modeling results suggest significant increases in the emissions from savanna, regrowing woods, and the rest of vegetations group. With a 52% increase of isoprene emissions to 51 Tg C yr$^{-1}$, the a posteriori model bias is decreased to −24.8% (Table 3).

[40] The model shows a small minimum in January when GOME observations show a maximum. The simulated decrease is due to a corresponding change in GEOS-STRAT surface temperature, which reduces isoprene emissions (not shown). A more prominent illustration of a similar problem over the northern equatorial African region is discussed in the next section. The European Centre for Medium-Range Weather Forecasts (ECMWF) surface temperature for the same period does not show this seasonal change, likely indicating a problem in GEOS-STRAT surface temperature simulation for this region.

### 5.2.9. Discrepancies Over Northern Equatorial Africa

[41] The largest discrepancy in the seasonal HCHO column variations between GOME observations and GEOS-CHEM simulations is found over northern equatorial Africa (4°–12°N). The dominant ecosystems over this region are savanna, tropical seasonal forest and thorn woods, drought deciduous, and grass/shrubs. The distributions and ecosystem types are different from other
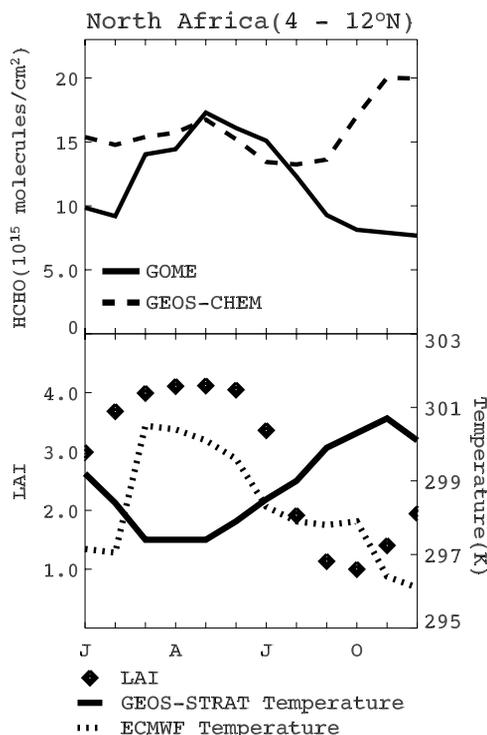
**Figure 7.** Discrepancy between monthly GOME-measured and GEOS-CHEM-simulated HCHO columns over northern equatorial Africa (4°–12°N). The corresponding monthly mean LAI, ECMWF surface temperature, and GEOS-STRAT surface temperature are shown in the lower panel. There are no GOME HCHO measurements that match our data selection criteria for inversion in November 1996 over this region.

African regions (Figure 2). This region is excluded in the inversion for Africa because of the large discrepancy between observed and simulated HCHO seasonal cycles. The GEOS-CHEM monthly mean HCHO columns show a seasonal maximum in November and December, whereas GOME shows a maximum in May (Figure 7). The monthly variations of the GEOS-STRAT and ECMWF surface temperature and GEOS-CHEM LAI for this region are also shown in Figure 7. The seasonal cycle of LAI is consistent with that of monthly GOME HCHO columns. However, the GEOS-STRAT surface temperature has an opposite seasonal cycle. In comparison, the seasonal cycle of the corresponding surface temperature simulated by ECMWF is consistent with GOME observations. Everything else being the same, isoprene emissions increase by 50% when temperature increases from 297 to 301 K.

[42] The GEIA emission inventory does not have the bias likely because the International Institute for Applied Systems Analysis (IIASA) monthly mean climatological surface temperature field [*Leemans and Cramer*, 1992] was used. For the same reason, *Wang et al.* [1998a] showed much lower isoprene emissions in January than July over northern equatorial Africa. The discrepancy appears to be caused by GEOS-STRAT overestimates of surface temperature for this region in fall and winter.

## 5.3. Degrees of Freedom of the Jacobian Matrix and Nonlinearity

[43] The state vector has a total of 12 source parameters in the inverse model. We selected only the parameters with significant contributions based on the a priori emissions because the noises introduced by small sources are sometimes manifested in the a posteriori results for significant sources. The resulting significant source parameters in the inversion are 7–9 for each region (Table 4). It is important to know if GOME HCHO measurements provide enough information to resolve these parameters. We evaluate the degree of freedom in inverse modeling by calculating the singular values of the prewhitened Jacobian matrix ($\overline{K} = S_\epsilon^{-1/2} K S_a^{1/2}$) [*Rodgers*, 2000; *Heald et al.*, 2004]; the degree of freedom is defined by the number of singular values >1. We find that GOME observations are generally enough to resolve the significant parameters in inverse modeling (Table 4) because the estimated number of significant parameters is close to the state vector size. The slightly large size of the state vector indicates some interdependence in the a posteriori estimates of source parameters.

[44] The sensitivities of the source parameters to HCHO columns in the inversion are assumed to be linear. We compare the linear projection of the inverse modeling with the a posteriori full chemistry simulation in Table 4. The largest nonlinearity of ∼8% is over Southeast Asia and Africa. The smallest nonlinearity of <2% is over North America and Europe. The other regions have a nonlinearity of 2–5%.

## 6. Effects of the Isoprene Emission Change on Global OH and O₃ Concentrations

[45] We extended the inverse modeling results (Table 3) to the adjacent continental regions (Figure 1) to estimate the isoprene emissions for each continent. We estimate the a posteriori global isoprene source of 566 Tg C yr⁻¹. It is ∼50% higher than that of the a priori source (375 Tg C yr⁻¹), and is slightly higher (12%) than the GEIA inventory of 503 Tg C yr⁻¹ [*Guenther et al.*, 1995]. The a posteriori global isoprene source is also comparable to that of 597 Tg C yr⁻¹ estimated by *Wang et al.* [1998a]. The a posteriori isoprene emissions from tropical rain forest and tropical seasonal forest are increased by ∼60% globally. When compared to the GEIA inventory, these emissions are lower (globally) by about 30% (Table 5). Therefore GOME HCHO observations support a general reduction of isoprene emissions from these tropical ecosystems but not as drastic as assumed in the a priori model. Of particular interest is that a posteriori isoprene emissions suggest that the reduction depends strongly on the continent. For example, the a posteriori reduction for the tropical rain forest emissions is a factor of 2.5 from GEIA over South America but is negligible over Africa (Table 5).

[46] Isoprene is the most dominant reactive VOC in the troposphere. The increase of isoprene emissions affects global tropospheric OH and O₃ concentrations [*Wang and Jacob*, 1998; *Spivakovsky et al.*, 2000]. Generally, the OH concentrations are reduced by reacting with isoprene and its oxidation products such as methyl vinyl ketone. The tropospheric annual mean OH concentration calculated by the a posteriori GEOS-CHEM simulation decreases by 10.8% to

**Table 4.** Samples, State Vector Size, Significant Eigenvalues, and Nonlinearity

|  | North America | Europe | East Asia | India | South Asia | South America | Africa | Australia |
|---|---|---|---|---|---|---|---|---|
| Samples[a] | 152 | 148 | 216 | 162 | 261 | 660 | 792 | 564 |
| State vector size[b] | 7 | 7 | 7 | 9 | 9 | 8 | 8 | 8 |
| Significant eigenvalues[c] | 6 | 5 | 6 | 6 | 8 | 7 | 7 | 6 |
| Nonlinearity,[d] % | 1.7 | 0.4 | 5.3 | 4.3 | 8 | 2.1 | 7.8 | 7.5 |

[a]The number of monthly mean GOME HCHO measurements that meet our criteria for the usage of inversion.
[b]The number of significant parameters (see text for details)
[c]The number of singular values of the prewhitened Jacobian that are >1.
[d]Calculated as [1 - (the a posteriori simulated HCHO column)/(inverse-model linearly projected HCHO column)] × 100.

$0.95 \times 10^6$ molecules/cm$^3$ resulting in an atmospheric methyl chloroform (CH$_3$CCl$_3$) lifetime against the tropospheric OH of 5.7 years (5.2 years for the a priori simulation), in better agreement with 5.99 (+0.95/−0.71) years estimated by *Prinn et al.* [2001]. The atmospheric CH$_3$CCl$_3$ lifetime is estimated in the same manner as *Bey et al.* [2001].

[47] The percent decreases of annual and zonal mean concentrations of OH and NO$_x$ due to the increase of the a posteriori isoprene and the other biogenic emissions are shown in Figure 8. The upper tropospheric reduction of OH in the tropics is due in part to convective transport of isoprene and its oxidation products to the region and in part to the significantly reduced NO$_x$ concentrations. The loss of NO$_x$ is due to the formation of PAN through the reaction of peroxyacetyl radicals and NO$_2$. Isoprene is a major precursor for peroxyacetyl radicals. The lifetime of PAN strongly depends on temperature. The effect is most significant in the upper troposphere, where low temperature leads to a long lifetime of PAN.

[48] The decrease of OH is also notable in the lower and upper troposphere at northern midlatitudes (30°−60°N). This is due to isoprene emissions over North America, Europe, and Siberia in summer. The impact of increased isoprene emissions on global tropospheric O$_3$ is much less than that of OH. The a posteriori tropospheric annual mean global O$_3$ burden increases only by 1.5% to 333 Tg.

## 7. Conclusions

[49] Atmospheric VOCs play an essential role in the tropospheric chemistry. Globally, isoprene accounts for a major fraction of the reactivity of VOCs. Current biogenic isoprene sources are highly uncertain because of limited in situ measurements, particularly over the tropics. We have presented the first Bayesian inverse modeling analysis of the global HCHO column measurements by GOME in order to evaluate the global isoprene emissions from September 1996 to August 1997. Different HCHO sources are explicitly taken into account in the inversion using GEOS-CHEM as the forward model.

[50] We selected eight regions with high signal-to-noise ratios in GOME measurements to conduct the inversion. To facilitate inverse modeling, we applied archived OH, NO, and O$_3$ concentrations from the standard simulation to estimate the sensitivities of HCHO columns to biogenic emissions from 10 vegetation groups, biomass burning, and industrial VOCs. The sensitivities are mostly linear in the range of emission changes in this study. The largest deviations of ∼8% from linearity are found over Southeast Asia and Africa.

[51] The a priori simulation greatly underestimates global HCHO columns over the eight regions (model bias, −14 to −46%; R = 0.52−0.84). The a posteriori results show generally higher isoprene and biomass-burning emissions. Comparison between the a priori and the a posteriori HCHO source parameters for the eight regions shows some general tendencies (Table 3). First, isoprene emissions from agricultural lands, tropical rain forest, tropical seasonal forest, and rest of the ecosystems are increased in almost all regions. Second, isoprene emissions from dry evergreen and crop/woods are reduced in most regions. Despite those tendencies, the a posteriori changes still depend on the continents. The HCHO sources from biomass-burning emissions are increased in all regions. The biomass-burning HCHO enhancements are >400% over South America and east Asia, >200% over Southeast Asia, and ∼50% over Africa. The a posteriori simulation improves the model bias for all regions (model bias, −3.6 to −25%; R = 0.56−0.84).

**Table 5.** Ratios of the a Posteriori Isoprene Base Emission Rates to Those of GEIA[a]

|  | North America | Europe | East Asia | India | South Asia | South America | Africa | Australia |
|---|---|---|---|---|---|---|---|---|
| V1 | - | - | - | 1.26 | 0.48 | 0.39 | 0.96 | - |
| V2 | 0.42 | 0.69 | 0.81 | 0.78 | - | 0.15 | 1.14 | 0.18 |
| V3 | - | - | - | - | - | 1.12 | 1.12 | 3.44 |
| V4 | - | - | - | - | 0.59 | 0.74 | 0.39 | - |
| V5 | 1.19 | 1.26 | 0.07 | - | 1.05 | - | - | 0.70 |
| V6 | 1.28 | 2.08 | 2.08 | 0.72 | 2.32 | - | - | 3.28 |
| V7 | 0.63 | 1.44 | - | 0.9 | - | 0.90 | - | 0.63 |
| V8 | 0.64 | 0.88 | 3.20 | 1.44 | 0.80 | - | 0.80 | 5.20 |
| V9 | - | - | - | 0.42 | 0.15 | 0.27 | 0.66 | 0.33 |
| RV | 1.04 | 0.88 | 1.36 | 1.92 | 2.56 | 1.44 | 2.08 | 1.76 |

[a]The definitions of vegetation types are listed in Table 3. Only vegetation groups included in the state vector are shown.
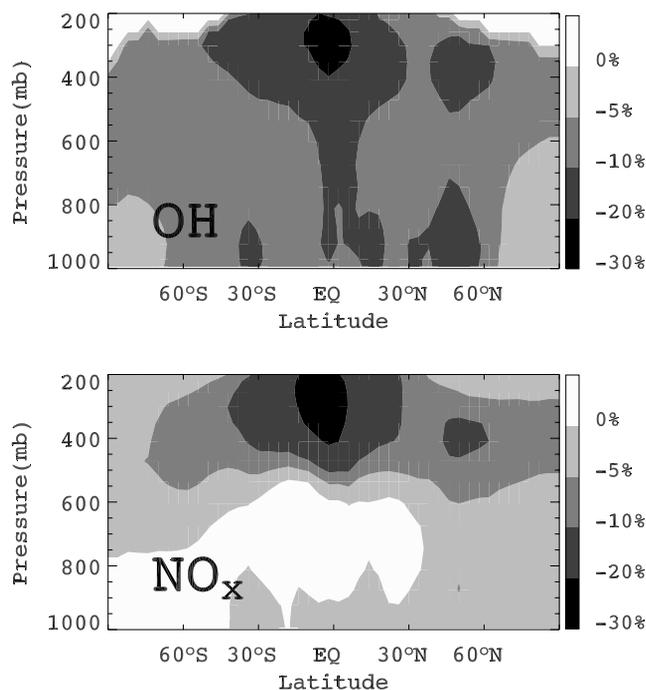
**Figure 8.** Percent changes of annual and zonal mean concentrations of OH and NO$_x$ due to the increase of the a posteriori isoprene and the other biogenic emissions.

[52] There is a significant discrepancy between the seasonality of GOME-measured and GEOS-CHEM-simulated HCHO columns over northern equatorial Africa. We attribute this problem to the incorrect seasonal cycle in surface temperature used in GEOS-CHEM. As a result, isoprene emissions over the region are overestimated. We also find that the model cannot reproduce the observed seasonal HCHO column increase from winter to summer over Southeast Asia and India. A major limitation of this study is due to the large uncertainties of the GOME HCHO column measurements resulting in relatively large uncertainties in the a posteriori emission estimates.

[53] The a posteriori estimate of the annual global isoprene emissions of 566 Tg C yr$^{-1}$ is about 50% larger than the a priori estimate. Table 5 shows the ratios of the a posteriori base emission rates to those of GEIA for different vegetation types and continents (the monthly mean a posteriori isoprene emissions are available at http://apollo.eas.gatech.edu/data/isoprene_05, and those data are also available in electronic format in the online auxiliary material[1]). The increase of global isoprene emissions significantly perturbs tropospheric chemistry, decreasing the global mean OH concentration by 10.8% from 1.06 to 0.95 $\times$ 10$^6$ molecules/cm$^3$ and increasing the tropospheric O$_3$ burden by 1.5% from 328 to 333 Tg. The atmospheric lifetime of CH$_3$CCl$_3$ increases from 5.2 to 5.7 years in closer agreement with the estimate by *Prinn et al.* [2001].

[54] We find that the a posteriori global isoprene annual emissions are generally higher at midlatitudes and lower in

the tropics when compared to the GEIA inventory [*Guenther et al.*, 1995]. The large reduction (a factor of 3) of isoprene emissions for some tropical ecosystems based on limited in situ measurements as used in the a priori simulations appears to be supported only for tropical rain forest in South America and tropical seasonal forest in Africa. Our results indicate large variations in the reduction factor ranging from 0 to 250% depending on region and ecosystem.

[55] In summary, the a posteriori results suggest higher isoprene emissions than a priori for agricultural lands, tropical rain forest, tropical seasonal forest, and rest of the ecosystems and lower isoprene base emissions for dry evergreen and crop/woods. The a posteriori biomass-burning HCHO sources increase by a factor of 2−4 in most regions with significant emissions except for India (only ∼10%). The industrial HCHO sources are higher by ∼20% except for east Asia and India (∼60%). Last, the a posteriori uncertainties of emissions, although greatly reduced, are still high (∼90%) reflecting the relatively large uncertainties in GOME retrievals. We did not include the kinetics uncertainty of HCHO yields from isoprene oxidation in the inversion. Further studies are merited on how to properly account for this uncertainty. Given the complexity of biogenic emissions and the enormous biodiversity in ecosystems, improved in situ measurements are likely to be available only for specific regions like North America and Europe, where the research capability and resources are up to this difficult task. On the global scale, however, more accurate HCHO or other proxy observations from the next generation satellites are necessary to improve the biogenic emission inventories.

## References

Abbot, D. S., P. I. Palmer, R. V. Martin, K. V. Chance, D. J. Jacob, and A. Guenther (2003), Seasonal and interannual variability of North American isoprene emissions as determined by formaldehyde column measurements from space, *Geophys. Res. Lett.*, 30(17), 1886, doi:10.1029/2003GL017336.

Andreae, M. O., and P. Merlet (2001), Emission of trace gases and aerosols from biomass burning, *Global Biogeochem. Cycles*, 15, 955−966.

Atkinson, R. (1994), Gas-phase tropospheric chemistry of organic compounds, *J. Phys. Chem. Ref. Data Monogr.*, 2, 13−46.

Bey, I., D. J. Jacob, R. M. Yantosca, J. A. Logan, B. D. Field, A. M. Fiore, Q. Li, H. Y. Liu, L. J. Mickley, and M. G. Schultz (2001), Global modeling of tropospheric chemistry with assimilated meteorology: Model description and evaluation, *J. Geophys. Res.*, 106, 23,073−23,096.

Burrows, J. P., et al. (1999), The Global Ozone Monitoring Experiment (GOME): Mission concept and first scientific results, *J. Atmos. Sci.*, 56, 151−175.

Carslaw, N., N. Bell, A. C. Lewis, J. B. McQuaid, and M. J. Pilling (2000), A detailed case study of isoprene chemistry during the EASE96 Mace Head campaign, *Atmos. Environ.*, 34, 2827−2836.

Chameides, W. L., et al. (1992), Ozone precursor relationship in the ambient atmosphere, *J. Geophys. Res.*, 97, 6037−6055.

Chance, K., P. I. Palmer, R. J. D. Spurr, R. V. Martin, T. P. Kurosu, and D. J. Jacob (2000), Satellite observations of formaldehyde over North America from GOME, *Geophys. Res. Lett.*, 27, 3461−3464.

Claeys, M., et al. (2004), Formation of secondary organic aerosols through photooxidation of isoprene, *Science*, 303, 1173−1176.

[1]Auxiliary material is available at ftp://ftp.agu.org/apend/jd/2004JD005629.

Dumdei, B. E., D. V. Kenny, P. B. Shepson, T. E. Kleindienst, C. M. Nero, L. T. Cupitt, and L. D. Claxton (1988), Ms/Ms analysis of the products of toluene photooxidation and measurement of their mutagenic activity, *Environ. Sci. Technol.*, 22(12), 1493–1498.

Duncan, B. N., R. V. Martin, A. C. Staudt, R. Yevich, and J. A. Logan (2003), Interannual and seasonal variability of biomass burning emissions constrained by satellite observations, *J. Geophys. Res.*, 108(D2), 4100, doi:10.1029/2002JD002378.

Guenther, A., et al. (1995), A global model of natural volatile organic compound emissions, *J. Geophys. Res.*, 100, 8873–8892.

Hatakeyama, S., K. Izumi, T. Fukuyama, H. Akimoto, and N. Washida (1991), Reactions of OH with α-pinene and β-pinene in air: Estimate of global CO production and atmospheric oxidation of terpenes, *J. Geophys. Res.*, 96, 947–958.

Heald, C. L., et al. (2004), Comparative inverse analysis of satellite (MOPITT) and aircraft (TRACE-P) observations to estimate Asian sources of carbon monoxide, *J. Geophys. Res.*, 109, D23306, doi:10.1029/2004JD005185.

Heirtzler, J. R. (2002), The future of the South Atlantic anomaly and implications for radiation damage in space, *J. Atmos. Sol. Terr. Phys.*, 64, 1701–1708.

Helmig, D., et al. (1998), Vertical profiling and determination of landscape fluxes of biogenic nonmethane hydrocarbons within the planetary boundary layer in the Peruvian Amazon, *J. Geophys. Res.*, 103, 25,519–25,532.

Hewitt, C. N., and R. Street (1992), A qualitative assessment of the emission of non-methane hydrocarbons from the biosphere to the atmosphere in the U.K.: Present knowledge and uncertainties, *Atmos. Environ., Part A*, 26, 3067–3077.

Horowitz, L. W., J. Liang, G. M. Gardner, and D. J. Jacob (1998), Export of reactive nitrogen from North America during summertime: Sensitivity to hydrocarbon chemistry, *J. Geophys. Res.*, 103, 13,451–13,476.

Houweling, S., F. Dentener, and J. Lelieveld (1998), The impact of non-methane hydrocarbon compounds on tropospheric photochemistry, *J. Geophys. Res.*, 103, 10,673–10,696.

Kamens, R. M., M. W. Gery, H. E. Jeffries, M. Jackson, and E. I. Cole (1982), Ozone-isoprene reactions: Product formation and aerosol potential, *Int. J. Chem. Kinet.*, 14, 955–975.

Klinger, L. F., J. Greenberg, A. Guenther, G. Tyndall, P. Zimmerman, M. M'Bangui, J. M. Moutsambot, and D. Kenfack (1998), Patterns in volatile organic compound emissions along a savanna rainforest gradient in central Africa, *J. Geophys. Res.*, 103, 1443–1454.

Kurosu, T. P., K. Chance, and R. J. D. Spurr (1999), GRAG: Cloud retrieval algorithm for the European Space Agency's Global Ozone Monitoring Experiment, in *Proceedings of the European Symposium of Atmospheric Measurements From Space*, pp. 513–521, Eur. Space Agency, Paris.

Lamb, B., A. Guenther, D. Gay, and H. Westberg (1987), A national inventory of biogenic hydrocarbon emissions, *Atmos. Environ.*, 21, 1695–1705.

Leemans, R., and W. P. Cramer (1992), IIASA database for mean monthly values of temperature, precipitation, and cloudiness on a global terrestrial grid, digital raster data on a 30 minute Cartesian orthonormal geodetic (lat/long) 360 × 720 grid, in *Global Ecosystems Database Version 2.0*, http://www.ngdc.noaa.gov/ngdc.html, NOAA Natl. Geophys. Data Cent., Boulder, Colo.

Limbeck, A., M. Kulmala, and H. Puxbaum (2003), Secondary organic aerosol formation in the atmosphere via heterogeneous reaction of gaseous isoprene on acidic particles, *Geophys. Res. Lett.*, 30(19), 1996, doi:10.1029/2003GL017738.

Martin, R. V., et al. (2002), An improved retrieval of tropospheric nitrogen dioxide from GOME, *J. Geophys. Res.*, 107(D20), 4437, doi:10.1029/2001JD001027.

Moxim, W. J., J. H. Levy II, and P. S. Kasibhatlan (1996), Simulated global tropospheric PAN: Its transport and impact on $NO_x$, *J. Geophys. Res.*, 101, 12,621–12,638.

Mueller, J.-F. (1992), Geographical distribution and seasonal variation of surface emissions and deposition velocities of atmospheric trace gases, *J. Geophys. Res.*, 97, 3787–3804.

Olson, J. (1992), World ecosystems (WE1.4), digital raster data on a 10 minute geographic 1080 × 2160 grid, in *Global Ecosystems Database, Version 1.0: Disc A*, http://www.ngdc.noaa.gov/ngdc.html, NOAA Natl. Geophys. Data Cent., Boulder, Colo.

Orlando, J. J., B. Nozière, G. S. Tyndall, G. E. Orzechowska, S. E. Paulson, and Y. Rudich (2000), Product studies of the OH-and ozone initiated oxidation of some monoterpenes, *J. Geophys. Res.*, 105, 11,561–11,572.

Palmer, P. I., D. J. Jacob, K. Chance, R. V. Martin, R. J. D. Spurr, T. P. Kurosu, I. Bey, R. Yantosca, A. Fiore, and Q. B. Li (2001), Air mass factor formulation for spectroscopic measurements from satellites: Application to formaldehyde retrievals from GOME, *J. Geophys. Res.*, 106, 14,539–14,550.

Palmer, P. I., D. J. Jacob, A. M. Fiore, R. V. Martin, K. Chance, and T. P. Kurosu (2003a), Mapping isoprene emissions over North America using formaldehyde column observations from space, *J. Geophys. Res.*, 108(D6), 4180, doi:10.1029/2002JD002153.

Palmer, P. I., D. J. Jacob, D. B. A. Jones, C. L. Heald, R. M. Yantosca, J. A. Logan, G. W. Sachse, and D. G. Streets (2003b), Inverting for emissions of carbon monoxide from Asia using aircraft observations over the western Pacific, *J. Geophys. Res.*, 108(D21), 8828, doi:10.1029/2003JD003397.

Pierce, T., C. Geron, L. Bender, R. Dennis, G. Tonnesen, and A. Guenther (1998), Influence of increased isoprene emissions on regional ozone modeling, *J. Geophys. Res.*, 103, 25,611–25,629.

Poisson, N., M. Kanankidou, and P. J. Crutzen (2000), Impact of non-methane hydrocarbons on tropospheric chemistry and the oxidizing power of the global troposphere: 3-dimensional modeling results, *J. Atmos. Chem.*, 36, 157–230.

Prinn, R., et al. (2001), Evidence for substantial variations of atmospheric hydroxyl radicals in the past two decades, *Science*, 292, 1882–1888.

Rodgers, C. D. (2000), *Inverse Methods for Atmospheric Sounding: Theory and Practice*, World Sci., Hackensack, N. J.

Schubert, S. D., R. B. Rood, and J. Pfaendtner (1993), An assimilated data set for Earth science applications, *Bull. Am. Meteorol. Soc.*, 105, 19,991–20,011.

Spivakovsky, C. M., et al. (2000), Three-dimensional climatological distribution of tropospheric OH: Update and evaluation, *J. Geophys. Res.*, 105, 8931–8980.

Spurr, R. J. D. (2002), Simultaneous derivation of intensities and weighting functions in a general pseudo-spherical discrete ordinate radiative transfer treatment, *J. Quant. Spectrosc. Radiat. Transfer*, 75, 129–175.

Wang, Y., and D. J. Jacob (1998), Anthropogenic forcing on tropospheric ozone and OH since preindustrial times, *J. Geophys. Res.*, 103, 31,123–31,135.

Wang, Y., D. J. Jacob, and J. A. Logan (1998a), Global simulation of tropospheric $O_3$-$NO_x$-hydrocarbon chemistry: 1. Model formulation, *J. Geophys. Res.*, 103, 10,713–10,726.

Wang, Y., D. J. Jacob, and J. A. Logan (1998b), Global simulation of tropospheric $O_3$-$NO_x$-hydrocarbon chemistry: 3. Origin of tropospheric ozone and effects of non-methane hydrocarbons, *J. Geophys. Res.*, 103, 10,757–10,767.

Zimmerman, P. (1979), Testing of hydrocarbon emissions from vegetation, leaf litter and aquatic surfaces, and development of a method for compiling biogenic emission inventories, *Rep. EPA-450-4-70-004*, U.S. Environ. Prot. Agency, Research Triangle Park, N. C.

————————
D. S. Abbot and P. I. Palmer, Department of Earth and Planetary Sciences, Harvard University, 20 Oxford Street, Cambridge, MA 02138, USA.

K. Chance, Harvard-Smithsonian Center for Astrophysics, 60 Garden Street, Cambridge, MA 02138, USA.

Y. Choi, C. Shim, and Y. Wang, Department of Earth and Atmospheric Sciences, Georgia Institute of Technology, 311 Ferst Drive, Atlanta, GA 30332-0340, USA. (cshim@eas.gatech.edu)